

Parametric Temporal Imaging

C. V. Bennett

Dept. of Electrical Engineering, University of California, Los Angeles, and
Lawrence Livermore National Laboratory, P.O. Box 808, L-174, Livermore, California, 94551
cvbennett@llnl.gov

and

B. H. Kolner

Dept. of Applied Science, 228 Walker Hall, University of California, Davis, Davis, California,
95616
kolner@leorg.ucdavis.edu

Parametric Temporal Imaging

C. V. Bennett

Dept. of Electrical Engineering, University of California, Los Angeles, and
Lawrence Livermore National Laboratory, P.O. Box 808, L-174, Livermore, California, 94551
cvbennett@llnl.gov

B. H. Kolner

Dept. of Applied Science, 228 Walker Hall, University of California, Davis, Davis, California, 95616
kolner@leorg.ucdavis.edu

Abstract: The operational principles and performance characteristics of parametric temporal imaging systems are discussed. In these systems the quadratic phase modulation of a time lens is realized through sum or difference frequency generation with a linearly chirped optical pump pulse. The imaging condition, magnification, and resulting image profile are presented for different mixing arrangements. Effects that limit the resolution and fidelity of the system are discussed. Experimental results of an upconversion time microscope achieving $103\times$ magnification, better than 178 fs resolution, and 5.7 ps field of view are presented.

OCIS codes: (320.7100) Ultrafast measurements; (320.7080) Ultrafast devices

Introduction

The choice of measurement technique used in characterizing ultrafast optical waveforms depends to a large extent on the nature of the waveform being measured as well as the information being sought (i.e. field magnitude, field phase, intensity, intensity autocorrelation, etc). No one technique is best suited to all cases and usually several are available in the laboratory. In this paper we present the principles and performance limitations of a relatively new measurement technique, based on temporal imaging [1–8], that allows for the magnification of optical waveforms to a time scale that is accessible to high speed photodiodes and sampling oscilloscopes. This approach bridges the domain of the sophisticated nonlinear optical techniques, applicable to subpicosecond phenomena, with the straightforward optoelectronic photon→charge-carrier→oscilloscope method common to almost all optical practice. We present the results of experiments with a time microscope that magnifies or rescales an arbitrary optical waveform by a factor of 103 with a resolution of better than 178 fs. The imaging system shows good fidelity in the imaging of a simple test waveform over an input field of view of 5.7 ps.

The principle of temporal imaging is based on the duality between the propagation behavior of the field envelopes in the problems of diffraction and dispersion. This is most easily seen when considering simplified descriptions of fields corresponding to the diffraction of a monochromatic beam bounded in the transverse direction and the dispersion of a pulsed plane wave of infinite transverse extent. For the diffraction problem, the total field can be described by the function

$$E(x, y, z, t) = E(x, y, z) \exp(i(\omega_0 t - kz)) \quad (1)$$

for a z -propagating beam where $E(x, y, z)$ governs the transverse beam profile in (x, y) as a function of the propagation distance z , and k is the wavenumber controlling the phase shift per-unit-distance

in the z -direction. Making the usual paraxial approximation, the envelope function $E(x, y, z)$ must satisfy the differential equation

$$\frac{\partial E}{\partial z} = -\frac{i}{2k} \left(\frac{\partial^2 E}{\partial x^2} + \frac{\partial^2 E}{\partial y^2} \right). \quad (2)$$

For the dispersion problem, we can describe the total electric field by the function

$$E(x, y, z, t) = A(z, t) \exp(i(\omega_0 t - \beta(\omega)z)) \quad (3)$$

which represents an infinite transverse plane wave propagating in the z -direction. $A(z, t)$ governs the amplitude profile in the direction of propagation and can represent a pulse or other waveform which evolves with the propagation distance z . The propagation constant $\beta(\omega)$ describes the medium's frequency dependent phase shift per-unit-distance. When the propagation constant can be accurately described over the bandwidth of the pulse by a series expansion to second order,

$$\beta(\omega) = \beta_0 + (\omega - \omega_0) \beta' + (\omega - \omega_0)^2 \frac{\beta''}{2}, \quad (4)$$

where

$$\beta_0 = \beta(\omega_0), \quad \beta' = \left. \frac{d\beta(\omega)}{d\omega} \right|_{\omega=\omega_0} = \frac{1}{v_g(\omega_0)}, \quad \text{and} \quad \beta'' = \left. \frac{d^2\beta(\omega)}{d\omega^2} \right|_{\omega=\omega_0}, \quad (5)$$

a partial differential equation for the envelope $A(z, t)$ can be obtained. The expression is further simplified by transforming to a coordinate system that is traveling with the mean group velocity of the pulse, $v_g(\omega_0)$. In the traveling-wave coordinate system,

$$\tau = (t - t_0) - \left(\frac{z - z_0}{v_g(\omega_0)} \right) \quad \text{and} \quad \xi = z - z_0, \quad (6)$$

where t_0 and z_0 are arbitrary references. With this transformation, the equation governing the evolution of the envelope $A(\xi, \tau)$ becomes

$$\frac{\partial A}{\partial \xi} = \frac{i\beta''}{2} \frac{\partial^2 A}{\partial \tau^2}. \quad (7)$$

Comparing equations (2) and (7) we see that paraxial diffraction and narrowband dispersion are governed by the same differential equations and thus admit similar solutions. The solution to either problem is most easily carried out in the frequency domain; either the spatial frequency spectrum of the transverse profile $\mathcal{E}(k_x, k_y, z) = \mathcal{F}\{E(x, y, z)\}$ or the angular frequency spectrum of the pulse envelope $\mathcal{A}(\xi, \omega) = \mathcal{F}\{A(\xi, \tau)\}$. In both cases the initial spectrum ($z, \xi = 0$) is multiplied by a quadratic phase factor;

$$E(x, y, z) = \frac{1}{(2\pi)^2} \iint_{-\infty}^{\infty} \mathcal{E}(k_x, k_y, 0) \exp\left(\frac{iz(k_x^2 + k_y^2)}{2k}\right) \exp(i(k_x x + k_y y)) dk_x dk_y \quad (8)$$

for the diffraction problem and

$$A(\xi, \tau) = \frac{1}{2\pi} \int_{-\infty}^{\infty} \mathcal{A}(0, \omega) \exp\left(\frac{-i\xi\beta''\omega^2}{2}\right) \exp(i\omega\tau) d\omega \quad (9)$$

for the dispersion problem. The quadratic phase factor is proportional to the propagation distance (z, ξ) in both cases and to $1/k$ for diffraction and β'' for dispersion. It's important to note that the group-velocity dispersion β'' may not be constant throughout a real dispersive delay line due to changes in the materials used. The dispersion may also be realized with angularly dispersive elements in which case β'' only has meaning for the whole dispersive network rather than as a distributed parameter. It is therefore often more useful to think of the propagation in terms of the total group-delay dispersion (GDD) that has been propagated through,

$$\phi'' = \sum_n \xi_n \beta_n'' = \left. \frac{d^2 \phi(\omega)}{d\omega^2} \right|_{\omega=\omega_0}, \quad (10)$$

for n regions with different dispersive characteristics.

A conventional space lens works by producing a quadratic phase transformation across the wavefront of a propagating wave. The strength of the lens action is proportional to k/f where f , the focal length, is the distance the wave must propagate beyond the lens to remove the imparted phase. In an analogous fashion, a time lens is any process that produces a quadratic phase modulation on a temporal waveform. The strength of this process is characterized by the chirp rate imparted by the lens $d\omega/d\tau = d^2\Phi(\tau)/d\tau^2$, where $\Phi(\tau)$ is the time lens phase function. A temporal focal length ξ_f can then be defined in terms of the GDD required to remove the quadratic phase modulation produced by the time lens. The GDD at the focal distance is $\phi_f'' \equiv \xi_f \beta'' \equiv -(d\omega/d\tau)^{-1}$ and the desired phase function of a time lens is given by

$$H(\tau) = \exp(i\Phi(\tau)) = \exp\left(\frac{-i\tau^2}{2\phi_f''}\right) \quad (11)$$

Temporal Imaging

When dispersion is followed by a time lens and then more dispersion, we have the temporal analog of a spatial imaging system consisting of diffraction followed by a space lens and more diffraction. Fully equivalent expressions for the imaging condition and magnification of an arbitrary time waveform can be derived [6] for a conventional temporal imaging system and are given by

$$\begin{array}{ll} \text{IMAGING CONDITION} & \text{MAGNIFICATION} \\ \frac{1}{\phi_1''} + \frac{1}{\phi_2''} = \frac{1}{\phi_f''} & M = -\frac{\phi_2''}{\phi_1''} \end{array} \quad (12)$$

where $\phi_1'' \equiv \xi_1 \beta_1''$ and $\phi_2'' \equiv \xi_2 \beta_2''$ are the total group-delay dispersions before and after the time lens, respectively.

The f -number of the time lens and thus the resolution of the temporal imaging system is inversely proportional to the bandwidth that is imparted by the modulation process; $f^\# = \omega_0/\Delta\omega$ [6]. The first optical time lenses used electro-optic phase modulators [9–15] but this technique has been unable to generate the bandwidth required to image modern ultrafast signals. Yet plenty of optical sources exist with the broad bandwidth desired of a good time lens, providing motivation for the parametric time lens technique [16–19]. In this approach, a broad bandwidth (ultrafast) optical pulse is linearly chirped by passage through a dispersive delay line and then mixed with the waveform being processed by the temporal imaging system. This imparts a linear chirp to the waveform and accomplishes the action required of a time lens.

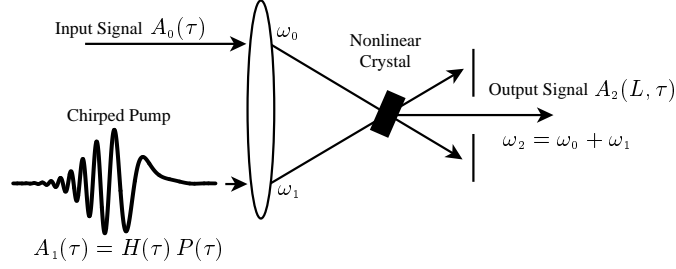


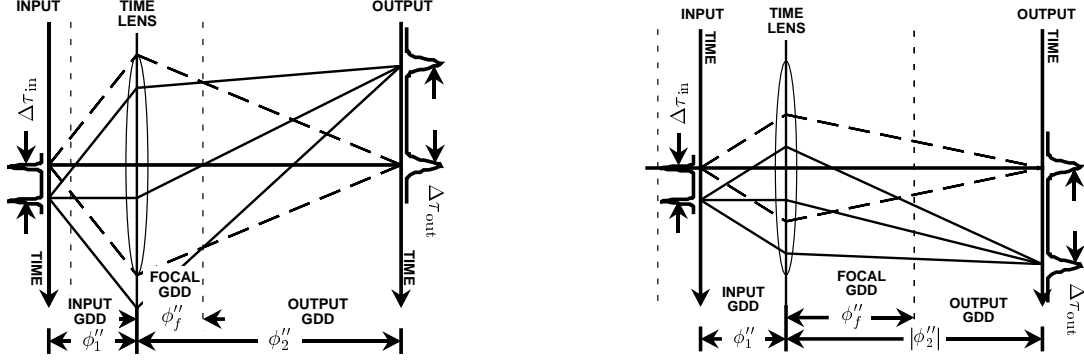
Fig. 1. An upconversion time lens. The output $A_2(\tau)$ is the product of the input signal $A_0(\tau)$ and chirped pump pulse $A_1(\tau)$. The phase profile of the pump, $H(\tau)$, is defined by (11). The pupil function, $P(\tau)$, is determined by the pump pulse amplitude profile.

An interesting aspect of the parametric time lens is that since there is no conversion in the absence of the pump pulse, the envelope of the pump effectively acts as a shutter or pupil function $P(\tau)$. For purposes of analysis it is convenient to separate this envelope function from the quadratic phase function $H(\tau)$ so that $A_1(\tau) = H(\tau)P(\tau)$. Another important point to realize is that both sum-frequency generation (SFG) and difference-frequency generation (DFG) can be used to impart a chirp. For consistency in the notation $H(\tau)$, and thus ϕ_f'' , will refer to the characteristics of the pump pulse even though the opposite chirp rate can be imparted by a DFG system.

Figure 1 shows a schematic diagram of the parametric time lens operating in an upconversion mode. The input signal $A_0(\tau)$ has arrived from the input dispersion having acquired a group-delay dispersion ϕ_1'' . It is combined in a nonlinear crystal with a linearly chirped pump $A_1(\tau)$. Under ideal phase matching conditions the SFG time lens radiates a new signal $A_2(\tau) \propto A_1(\tau)A_0(\tau)$ at a new carrier frequency $\omega_2 = \omega_1 + \omega_0$. The sum-frequency signal $A_2(\tau)$ is passed on to the output dispersive delay line where it acquires an additional group-delay dispersion, ϕ_2'' , in accord with the imaging condition (12).

The governing equations for a SFG system are identical to those in the general development of temporal imaging presented in [6] since SFG does not modify the envelope functions involved and the change in carrier frequency only affects the frequency at which the dispersions are evaluated. Imaging with a DFG time lens will introduce a complex conjugate to the development, with the output of the nonlinear crystal given by either $A_2(\tau) \propto A_1(\tau)A_0^*(\tau)$ at $\omega_2 = \omega_1 - \omega_0$ or $A_2(\tau) \propto A_1^*(\tau)A_0(\tau)$ at $\omega_2 = \omega_0 - \omega_1$ depending on the phase matching geometry. The complex conjugate is introduced in the middle of the imaging system and thus necessitates a change in the imaging condition. Following the procedure presented in [6] it can be shown that a ‘‘Pump–Input’’ temporal imaging system requires $-1/\phi_1'' + 1/\phi_2'' = 1/\phi_f''$ to be properly focussed and produces a magnification $M = +\phi_2''/\phi_1''$. An ‘‘Input–Pump’’ system requires $1/\phi_1'' + 1/\phi_2'' = -1/\phi_f''$ and results in a magnification $M = -\phi_2''/\phi_1''$.

The temporal images produced by these systems are all very similar. There are changes in the phase of the resulting images but the intensity profiles would be identical. It is interesting to note that in all cases there is a chirp remaining in the temporal image that is equal to the chirp of the pump pulse divided by the magnification. Unlike diffraction, which always introduces a positive spatial chirp for a forward traveling signal, GDD can be either positive or negative. This dual sign nature of dispersion leads to extra flexibility in configuring a temporal imaging system and allows a single lens temporal system to be constructed having either positive or negative magnification. For the SFG case we see that $\phi_1''/\phi_f'' \gtrsim 1$ results in a large negative magnification and $\phi_1''/\phi_f'' \lesssim 1$



(a) System with magnification $M = -3$. All GDD must be the same sign.

(b) System with magnification $M = +3$. Output must have opposite sign of input and focal GDD.

Fig. 2. Temporal ray diagrams. Note: Vertical axis in both figures is local time. Horizontal axis is propagation distance in units of GDD.

results in a large positive magnification, as shown graphically in Fig. 2. For the Pump–Input case it is found that $\phi_1''/\phi_f'' \gtrsim -1$ produces a large positive magnification and $\phi_1''/\phi_f'' \lesssim -1$ produces a large negative magnification. The same is true for the Input–Pump case.

Temporal ray diagrams [20] are a useful aid for understanding the temporal imaging process. Consider a SFG temporal imaging system and the two possible imaging configurations depicted in Fig. 2. The ordinate (vertical axis) is the local time relative to the group delay $\tau_g(\omega_0) = \xi/v_g(\omega_0) = \xi[d\beta(\omega)/d\omega]_{\omega=\omega_0}$ of a spectral packet centered at $\omega = \omega_0$. Any other spectral packet centered at another frequency ω will propagate with a group velocity $v_g(\omega)$ and arrive with a group delay $\tau_g(\omega) = \xi/v_g(\omega) = \xi d\beta(\omega)/d\omega$. The difference in the group delays between these packets traces out the rays in the temporal ray diagrams and depends on the frequency dependence of the group velocity (dispersion). If this dispersion is a linear function of frequency, then we may write

$$\Delta\tau(\omega) = \tau_g(\omega) - \tau_g(\omega_0) \quad (13)$$

$$= (\omega - \omega_0)\xi \left[\frac{d}{d\omega} \left(\frac{1}{v_g} \right) \right]_{\omega=\omega_0} \quad (14)$$

$$= (\omega - \omega_0)\xi\beta'' \quad (15)$$

The abscissa (horizontal axis) is the group delay dispersion $\phi'' = \xi\beta''$ in the region of interest. Thus, the slope of a particular ray corresponding to a spectral packet centered at $\omega = \omega_0$ in a linearly dispersive region is given by

$$\frac{\Delta\tau(\omega)}{\phi''} = \frac{(\omega - \omega_0)\xi\beta''}{\xi\beta''} = (\omega - \omega_0). \quad (16)$$

The effect of higher order dispersion would cause the rays to follow curved trajectories in the temporal ray diagrams.

The familiar imaging system configuration with negative magnification is shown in Fig. 2(a) and requires all GDD to be of the same sign, with $\phi_1''/\phi_f'' > 1$. The only difference between positive and negative dispersive systems would be whether a ray increasing in time corresponded to positive spectral components $\omega - \omega_0 > 0$ propagating through positive dispersion $\phi'' > 0$ or a negative spectral component $\omega - \omega_0 < 0$ propagating through negative dispersion $\phi'' < 0$. To produce the positive magnification shown in Fig. 2(b) requires $0 < \phi_1''/\phi_f'' < 1$ and an output GDD ϕ_2''

with the opposite sign as the input and focal GDD, analogous to virtual imaging systems in space except that the signal is still propagating forward in space and comes out of the system as a real measurable image. Both figures show two pulses at the same carrier frequency spreading as they propagate through the input GDD. The phase modulation process in the time lens frequency shifts each spectral component (ray) causing them to appear bent. The output GDD then focuses the rays creating a temporally scaled image.

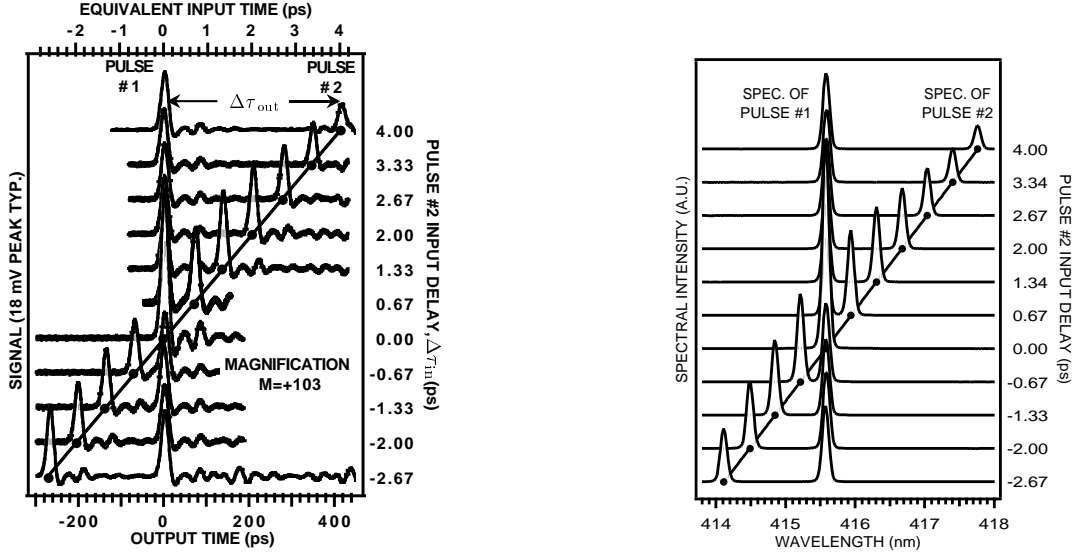
Resolution and Temporal Aberrations

In a real system the parametric interaction only transmits a phase modulated signal over the duration of the pump profile $P(\tau)$. It was shown in [6] that the ideal response of a temporal imaging system to an input impulse at τ_0 is given by

$$\tilde{h}(\tau - \tilde{\tau}_0) = \frac{1}{2\pi\phi_2''\sqrt{M}} \exp\left(\frac{-i\tau^2}{2M\phi_f''}\right) \int_{-\infty}^{+\infty} P(\tau') \exp\left[\frac{-i\tau'(\tau - \tilde{\tau}_0)}{\phi_2''}\right] d\tau', \quad (17)$$

where $\tilde{\tau}_0 = M\tau_0$. Thus we see that the impulse response is given by the Fourier transform of the pump profile in a scaled and shifted coordinate system. One possible definition of the resolution of a temporal imaging system is that two pulses are “resolved” when they are separated at the output by the width of the system’s impulse response. For a Gaussian time lens pump pulse with perfectly linear frequency chirp and this definition of resolution it can be shown that the resolution referred to the input is $\delta\tau_{\text{in}} = .44T f^\#$ or $\delta\tau_{\text{in}} \Delta f_{\text{pump}} = .44$ where T is an optical period and Δf_{pump} is the bandwidth of the pump. This definition of resolution may not be suitable for all applications but it shows that if our pump pulse is a dispersed pulse that was initially transform limited at around 100 fs it is reasonable to expect a temporal imaging system resolution near 100 fs. It can also be shown that for a system with large magnification and an input signal having a bandwidth comparable to that of the time lens pump the field of view will be approximately equal to the duration of the pump profile. Thus the number of resolvable temporal features for a parametric time microscope is approximately the amount the pump pulse has been stretched from its transform limit.

Efficient conversion of each spectral component of the input waveform requires phase and group velocity matching of all three signals in the crystal. While there are well established methods for matching the phase velocities of signals in anisotropic nonlinear crystals, there may be nothing that can be done about the group velocity mismatch. An extensive analysis has been done on phase and group velocity mismatch effects for pulsed second-harmonic generation [21] and sum-frequency generation [22]. These analyses are directly applicable to SFG temporal imaging. When this effect is included in a temporal imaging system it can be shown to produce a complicated spectral filtering [17] which acts as an aberration in the imaging system. In the particular case where the carrier of the pump is the same as that of the signal, $\omega_1 = \omega_0$, and Type I noncollinear phase matching is used, the result simplifies to a spectral filter at the output of the imaging system. The actual impulse response in this case is given by the ideal expression in (17) convolved with a rectangular pulse with duration equal to the difference in group delay of the fundamental and second harmonic in propagating through the crystal. This bandwidth filtering leads to an increase in the width of the system’s impulse response and because of the chirp across the temporal image an additional source of roll-off in the field of view. Since the conversion efficiency and this blurring effect are both directly proportional to the interaction length in the crystal a trade-off must be made.



(a) Temporal images. For each 667 fs step in the input delay of Pulse #2, $\Delta\tau_{in}$, a corresponding output delay, $\Delta\tau_{out}$, of 68.7 ps was observed, indicating a magnification of $M = +103$.

(b) Output spectra. Linear frequency shift and symmetric spectral profile show no signs of significant input or lens aberrations.

Fig. 4. Measured output temporal image and spectrum vs. input delay of Pulse #2.

produced a time lens with an f -number of 82. The input and output GDDs were also realized with folded multipass grating-pair dispersive delay lines, though a curved mirror was used in the input to change the sign of the GDD [23, 24]. Both the input and pump dispersions used 600 g/mm gratings. The dispersions were characterized using “Spectrally Resolved Up-Conversion” [25] and resulted in $\phi_1'' = +0.17606 \text{ ps}^2$, and a time lens with focal GDD $\phi_f'' = +0.17784 \text{ ps}^2$. The output GDD used a 3600 g/mm grating and was configured for $\phi_2'' = -17.606 \text{ ps}^2$.

Figure 4(a) shows a series of temporal images recorded with a 40 GHz photodiode and sampling oscilloscope. The output spectrum for each temporal image was also recorded and is shown in the adjacent Fig. 4(b). Between each measurement the delay of pulse #2 was increased by $100.0 \pm 0.1 \mu\text{m}$ or 667 fs round trip. The right vertical axis in Figs. 4(a) and 4(b) is the input delay of the #2 pulse corresponding to each recorded output. The bottom axis in Fig. 4(a) is the actual photodiode signal time scale. A linear fit to the output vs. input time of pulse #2 gives a magnification of $M = +103$ with an error of 22 fs rms referred to the input. The top scale in Fig. 4(a) is an equivalent input timescale found by dividing the output time by the measured magnification. Temporal images were also recorded in 100 fs delay steps near $\Delta\tau_{in} = 0 \text{ fs}$, and are shown in Fig. 5. For delays as short as $\Delta\tau_{in} = 300 \text{ fs}$ two pulses are still clearly resolved in the temporal image. For shorter delays the actual input waveform is determined by the interference of the two overlapping input pulses. This is demonstrated by the constructive interference recorded at $\Delta\tau_{in} = 0 \text{ ps}$ in Fig. 4(a) and the destructive interference recorded at $\Delta\tau_{in} = 0 \text{ ps}$ in Fig. 5. Between these two measurements a $0.7 \text{ fs} \pm 0.7 \text{ fs}$ ($\lambda/4 \pm \lambda/4$) change in the delay of pulse #2 from the Michelson interferometer test pattern generator was made. The interference and uncertainty in the path length change ($\pm\lambda/4$) leaves what is resolvable open to interpretation.

The resolution and fidelity of the total system not only depends on the quality of the temporal imaging system but also on the final recording device. The impulse response of the photodiode is 12.5 ps FWHM, with some ringing. The distortion this produces is clearly observed in Fig. 4(a) but

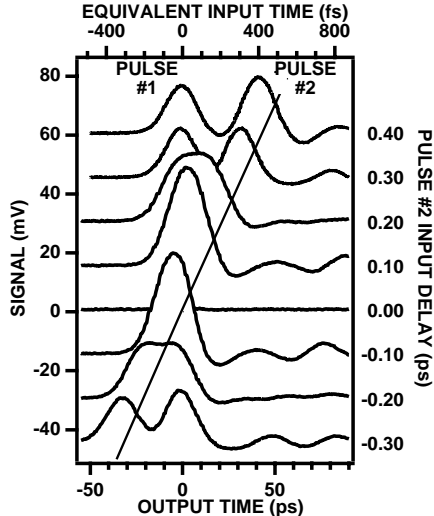


Fig. 5. Temporal images of two input pulses with 100 fs steps in the input time of pulse #2. The straight line corresponds to a magnification of $M = +103$.

it is **not** the result of aberrations in the temporal imaging system itself. From a convolution of the ideal image, the ideal impulse response of the imaging system, and the measured impulse response of the photodiode, a 17.8 ps output pulse width was expected. The average measured width of pulse #2 in the images is 18.3 ps. Using the resolution criteria discussed earlier, and noting that the input pulses in this experiment are not short enough to approximate an impulse, it suggests a system input resolution better than 178 fs.

The expected roll-off in the field of view is not readily apparent in Fig. 4(a). This could be masked by slight mechanical instabilities affecting the coupling into the photodiode. The spectral data of Fig. 4(b) clearly shows a Gaussian roll-off in the peak spectral intensity of pulse #2 as a function of input time, a fit to which gives an input temporal field of view of 5.65 ps FWHM, and is in good agreement with the width of the chirped time lens pump pulse.

Summary

In conclusion, we have discussed many of the fundamental principles and performance issues for a parametric temporal imaging system. The time lens in these systems is implemented by mixing the input signal with a chirped optical pump pulse. An upconversion time microscope has been demonstrated with $+103\times$ magnification and better than 178 fs resolution. In addition, since a time microscope produces an expanded replica of the full field of view of the input waveform without the use of sampling, it should be suitable for extending the range of single-shot waveform recording with optical streak cameras. It is expected that a scaling of this technology will lead to the realization of a new class of long record length, single transient recorders with ultrafast resolution.

Acknowledgments

This work was supported in part by the U.S. Department of Energy’s Lawrence Livermore National Laboratory under contract No. W-7405-Eng-48, the LLNL Photonics Group under LDRD grant No. 98-ERD-027, the National Science Foundation, the ATRI program of the US Air Force, and the David and Lucile Packard Foundation.

References

1. P. Tournois, J.-L. Verner, and G. Bienvenu, "Sur l'analogie optique de certains montages électroniques: Formation d'images temporelles de signaux électriques," *C. R. Acad. Sci.*, vol. 267, pp. 375–378, 1968.
2. W. J. Caputi, "Stretch: A time transformation technique," *IEEE Trans. Aerosp. Electron. Syst.*, vol. AES-7, pp. 269–278, 1971.
3. L. S. Telegin and A. S. Chirkin, "Reversal and reconstruction of the profile of ultrashort light pulses," *Sov. J. Quantum Electron.*, vol. 15, pp. 101–102, 1985.
4. S. A. Akhmanov, V. A. Vysloukh, and A. S. Chirkin, "Self-action of wave packets in a nonlinear medium and femtosecond laser pulse generation," *Sov. Phys. Usp.*, vol. 29, pp. 642–677, 1987.
5. B. H. Kolner and M. Nazarathy, "Temporal imaging with a time lens," *Opt. Lett.*, vol. 14, pp. 630–632, 1989, and erratum vol. 15, p. 655, 1990.
6. B. H. Kolner, "Space-time duality and the theory of temporal imaging," *IEEE J. Quantum Electron.*, vol. 30, pp. 1951–1963, Aug. 1994.
7. P. Naulleau and E. Leith, "Stretch, time lenses, and incoherent time imaging," *Appl. Opt.*, vol. 34, no. 20, pp. 4119–4128, 1995.
8. Prof. Kolner's Laser and Electro-optic Research Group, University of California, Davis, <http://www.engr.ucdavis.edu/~leorg/>.
9. J. A. Giordmaine, M. A. Duguay, and J. W. Hansen, "Compression of optical pulses," *IEEE J. Quantum Electron.*, vol. QE-4, pp. 252–255, 1968.
10. D. R. Grischkowsky, "Optical pulse compression," *Appl. Phys. Lett.*, vol. 26, pp. 566–568, 1974.
11. J. K. Wigmore and D. R. Grischkowsky, "Temporal compression of light," *IEEE J. Quantum Electron.*, vol. QE-14, pp. 310–315, 1978.
12. B. H. Kolner, "Active pulse compression using an integrated electro-optic phase modulator," *Appl. Phys. Lett.*, vol. 52, no. 14, pp. 1122–1124, 1988.
13. A. A. Godil, B. A. Auld, and D. M. Bloom, "Picosecond time-lenses," *IEEE J. Quantum Electron.*, vol. 30, no. 3, pp. 827–837, 1994.
14. B. H. Kolner, C. V. Bennett, and R. P. Scott, "Space-time duality and temporal imaging," in *Proc. SPIE OE/LASE*, vol. 2116, 1994. Paper 37.
15. M. T. Kauffman, A. A. Godil, W. C. Banyai, and D. M. Bloom, "Applications of time lens optical systems," *Electronics Letters*, vol. 29, pp. 268–269, 1993.
16. C. V. Bennett, R. P. Scott, and B. H. Kolner, "Temporal magnification and reversal of 100 Gb/s optical data with an up-conversion time microscope," *Appl. Phys. Lett.*, vol. 65, pp. 2513–2515, Nov. 1994.
17. C. V. Bennett, "Temporal magnification and reversal of 100 Gb/s optical data using an up-conversion time lens," Master's thesis, University of California, Los Angeles, 1995.
18. E. Arons, E. N. Leith, A.-C. Tien, and R. Wagner, "High-resolution optical chirped pulse gating," *Appl. Opt.*, vol. 36, no. 12, pp. 2603–2608, 1997.
19. C. V. Bennett and B. H. Kolner, "Upconversion time microscope demonstrating $103\times$ magnification of femtosecond waveforms," *Opt. Lett.*, vol. 24, no. 11, June 1, 1999 (to be published).
20. S. P. Djaili, A. Dienes, and J. S. Smith, "ABCD matrices for dispersive pulse propagation," *IEEE J. Quantum Electron.*, vol. 26, pp. 1158–1164, June 1990.
21. A. M. Weiner, "Effect of group velocity mismatch on the measurement of ultrashort optical pulses via second harmonic generation," *IEEE J. Quantum Electron.*, vol. QE-19, pp. 1276–1283, Aug. 1983, and erratum vol. QE-20, no. 8, p. 449, April 1984.
22. A. P. Baronavski, H. D. Ladouceur, and J. K. Shaw, "Analysis of cross correlation, phase velocity mismatch, and group velocity mismatches in sum-frequency generation," *IEEE J. Quantum Electron.*, vol. 29, pp. 580–589, Sept. 1993.
23. E. B. Treacy, "Optical pulse compression with diffraction gratings," *IEEE J. Quantum Electron.*, vol. QE-5, pp. 454–458, 1969.
24. O. E. Martinez, J. P. Gordon, and R. L. Fork, "Negative group-velocity dispersion using refraction," *J. Opt. Soc. Am. A*, vol. 1, pp. 1003–1006, 1984.
25. J.-P. Foing, J.-P. Likforman, M. Joffre, and A. Migus, "Femtosecond pulse phase measurement by spectrally resolved up-conversion: application to continuum compression," *IEEE J. Quantum Electron.*, vol. 28, pp. 2285–2290, Oct. 1992.